Top Catal (2012) 55:723–730
DOI 10.1007/s11244-012-9873-4

ORIGINAL PAPER

Reforming of C_6 Hydrocarbons Over Model Pt Nanoparticle Catalysts

Selim Alayoglu · Vladimir V. Pushkarev · Nathan Musselwhite · Kwangjin An · Simon K. Beaumont · Gabor A. Somorjai

Published online: 28 July 2012

Abstract Size-controlled model Pt nanoparticle catalysts, synthesized by colloidal chemistry, were used to study the hydrogenative reforming of three C_6 hydrocarbons in mixtures with 5:1 excess of H_2: methylcyclopentane, *n*-hexane and 2-methylpentane. We found a strong particle size dependence on the distribution of different reaction products for the hydrogenolysis of methylcyclopentane. The reactions of 50 Torr methylcyclopentane in 250 Torr H_2 at 320 °C, using 1.5 and 3.0 nm Pt nanoparticles produced predominantly C_6 isomers, especially 2-methylpentane, whereas 5.2 and 11.3 nm Pt nanoparticles were more selective for the formation of benzene. For the hydrogenolysis of n-hexane and 2-methylpentane, strong particle size effects on the turnover rates were observed. Hexane and 2-methylpentane reacted up to an order of magnitude slower over 3.0 nm Pt than over the other particle sizes. At 360 °C the isomerization reactions were more selective than the other reaction pathways over 3.0 nm Pt, which also yielded relatively less benzene.

S. Alayoglu · V. V. Pushkarev · N. Musselwhite · K. An · S. K. Beaumont · G. A. Somorjai (✉)
Department of Chemistry, University of California, Berkeley, Berkeley, CA, USA
e-mail: somorjai@berkeley.edu

S. Alayoglu · V. V. Pushkarev · N. Musselwhite · K. An · S. K. Beaumont · G. A. Somorjai
Chemical Sciences Division, Lawrence Berkeley National Laboratory, Berkeley, CA, USA

V. V. Pushkarev
Corning Corp., 2200 Salzburg Rd., Midland, MI 48686, USA

S. K. Beaumont
Department of Chemistry, Durham University, South Road, Durham DH1 3LE, UK

Keywords Pt nanoparticles · Size-control · Hydrogenative reforming · Methylcyclopentane n-Hexane · 2-Methylpentane

1 Introduction

Structure-sensitive multi-product reactions such as the hydrogenation of crotonaldehyde, pyrrole and furan show strong dependence of reactivity on particle size and/or shape over Pt crystals and nanoparticles. [1–5] Hence, model nanoparticle catalysts with well-defined structural and chemical properties such as particle size, morphology, crystallographic orientation, and redox state offer a unique way of assessing surface reactivity and reaction mechanisms for heterogeneous metal-catalyzed hydrocarbon transformations. The hydrogenative reforming of C_6 hydrocarbons are multi-path and multi-product reactions, which yield C_6 isomers (i.e. hexane and its derivatives) via hydrogenative ring opening/skeletal re-arrangement [6–12], benzene via ring enlargement/closure and aromatization [11–14], as well as shorter chain hydrocarbons (i.e. C_1–C_5 isomers) via hydrogenolysis cracking [15, 16]. Pt catalysts have been reported to be selective for the formation of branched hexane derivatives (i.e. 2-methylpentane and 3-methylpentane) during the reforming of methylcyclopentane [6, 7, 17–20]. Recently, we documented the strong correlation between the Pt particle morphology and catalytic reactivity for reactions of 10 Torr methylcyclopentane and 50 Torr H_2 at 240 °C [21]. We found that ~6 nm Pt nanoparticles with spherical, cubo-octahedral, octahedral and cubic morphologies (and the corresponding crystallographic shapes) exhibited distinct surface dependant reactivity during this catalytic reaction.

In this paper, we focus on the hydrogenative reforming reactions of three C_6 hydrocarbons - methylcyclopentane, hexane and 2-methylpentane - over model Pt nanoparticle catalysts with Pt particle size in the range between 1.5 and 11.3 nm. The catalytic reactivity of well-characterized Pt nanoparticles is evaluated under 50 Torr hydrocarbon and 250 Torr H_2, and in the temperature range of 280–360 °C. We find a strong correlation between the surface reactivity and the Pt particle size for these C_6 hydrocarbon transformations. For the hydrogenolysis of methylcyclopentane at 320 °C, Pt nanoparticle sizes of 3.0 nm and below lead to the production of C_6 alkanes via isomerization, specifically 2-methylpentane, while nanoparticle sizes of 5.2 nm and above yield the formation of benzene via ring enlargement and aromatization. For the hydrogenative reforming of the acyclic alkanes: hexane and 2-methylpentane, we isolate a rather weak particle size dependence on the product distribution. At 360 °C, 3.0 nm Pt nanoparticles isomerize both hexane and 2-methylpentane to 3-methylpentane more selectively than any other size of Pt nanoparticles. However, 3.0 nm Pt nanoparticles perform poorly for the conversion of C_6 alkanes (4–10 times diminished) as compared to 1.5 and 5.2 nm Pt nanoparticles.

2 Experimental

2.1 Material Preparation and Characterization

Polyvinylpyrrolidone (PVP)-capped Pt nanoparticles with average particle sizes of 1.5 ± 0.26, 3.0 ± 0.45, 5.2 ± 0.68 and 11.3 ± 1.10 nm were synthesized and supported in mesoporous silica (SBA-15 or MCF-17) according to the previously reported protocols [21]. Typically, $Pt(acac)_2$ (acac=acetylacetonate) and/or H_2PtCl_6 precursor salts were dissolved in alcohols (i.e. methanol or ethylene glycol) in the presence of PVP, and reacted at boiling solvent temperatures. The as-synthesized nanoparticles were washed and redispersed in chloroform. To prepare the supported catalysts, nanoparticle colloids were mixed with mesoporous silica support giving a nominal metal loading of 1 wt%. The mixtures were sonicated for 1 h, and then supported nanoparticle catalysts were collected by centrifugation. To remove excess PVP, nanoparticle catalysts were washed in 20 vol% ethanol in acetone 7 times. The 1.5 and 5.2 nm Pt nanoparticles were supported on SBA-15 (with an average pore size of 9.5 nm), while MCF-17 (with pore sizes in the range of 20–50 nm) was used to support the 11.3 nm Pt nanoparticles. Both SBA-15 and MCF-17 were used separately to support the 3.0 nm Pt nanoparticles and similar catalytic activities and selectivities were obtained for the resulting supported catalysts. As-synthesized nanoparticles were characterized by TEM (Jeol 2100 LaB_6). The supported catalysts were characterized by inductively coupled plasma atomic emission spectroscopy, (ICP-AES), ethylene hydrogenation, and TEM (Jeol 2100-FE) and reported elsewhere [21]. Turnover rates were calculated from the measured reaction rates and comparison with the number of active surface sites as obtained by using ethylene hydrogenation as a probe reaction to titrate the surface sites.

2.2 Catalytic Testing

The catalytic testing was performed using our home-built plug-flow reactor connected to a Hewlett Packard 5890 gas chromatograph. A 10 % SP-2100 on 100/120 supelcoport packed column in line with a FID detector was used to separate and analyze the C_1–C_6 hydrocarbons. Mass flow controllers were carefully calibrated using a bubble flowmeter and used to introduce the ultra high purity (99.9999 % Praxair) H_2 and He gases. Saturated vapor pressure C_6 hydrocarbons (methylcyclopentane, GC grade Aldrich; *n*-hexane, ReagentPlus® ≥99 % Aldrich; and 2-methylpentane, ≥99 % Aldrich) at room temperature (23 °C) were introduced to the reactor using a bubbler. The reactant flow was carefully calibrated at different temperatures and partial pressures of He carrier. A total flow of 40 ml/min was used. Total pressure under flow conditions, measured by using a Baratron capacitance gauge located above the reactor bed, was 790 Torr. Partial pressure of reactants was calculated by using the known temperature vs. saturated vapor pressure plots and was 50 Torr with 5:1 H_2 excess. 100–250 mg charges of the catalysts were diluted by quartz sand with average granular size of 0.4 mm and loaded in the reactor bed. The actual weight of catalyst used was selected to give similar total conversions in each case. The catalysts were reduced at 260 °C for 2 h under a flow of 210 Torr H_2 in 550 Torr He prior to catalytic testing. The catalytic activity and selectivity were evaluated for total conversions below 5 %.

3 Results

Size controlled Pt nanoparticles have been evaluated for the hydrogenolysis of three C_6 hydrocarbons to investigate possible reforming reaction pathways. For this, 50 Torr of any C_6 hydrocarbon in a mixture with 250 Torr H_2 was reacted at temperatures between 280 and 360 °C over Pt nanoparticles with the average particle sizes of 1.5 ± 0.26, 3.0 ± 0.45, 5.2 ± 0.68 and 11.3 ± 1.10 nm. Figure 1 shows the representative TEM pictures of the post-reaction Pt nanoparticle catalysts. As-synthesized nanoparticles, and

pre- and post-reaction nanoparticle catalysts are polyhedral in shape and nanocrystalline. The selectivities for the different reaction pathways, namely isomerization, cyclization (and/or dehydrogenation to cyclic olefins), aromatization and cracking, were plotted at 280 °C (low temperature), 320 °C (intermediate temperature) and 360 °C (high temperature) for methylcyclopentane (MCP), 2-methylpentane (2-MP) and *n*-hexane (Hex) in Figs. 2, 3, 4, for the

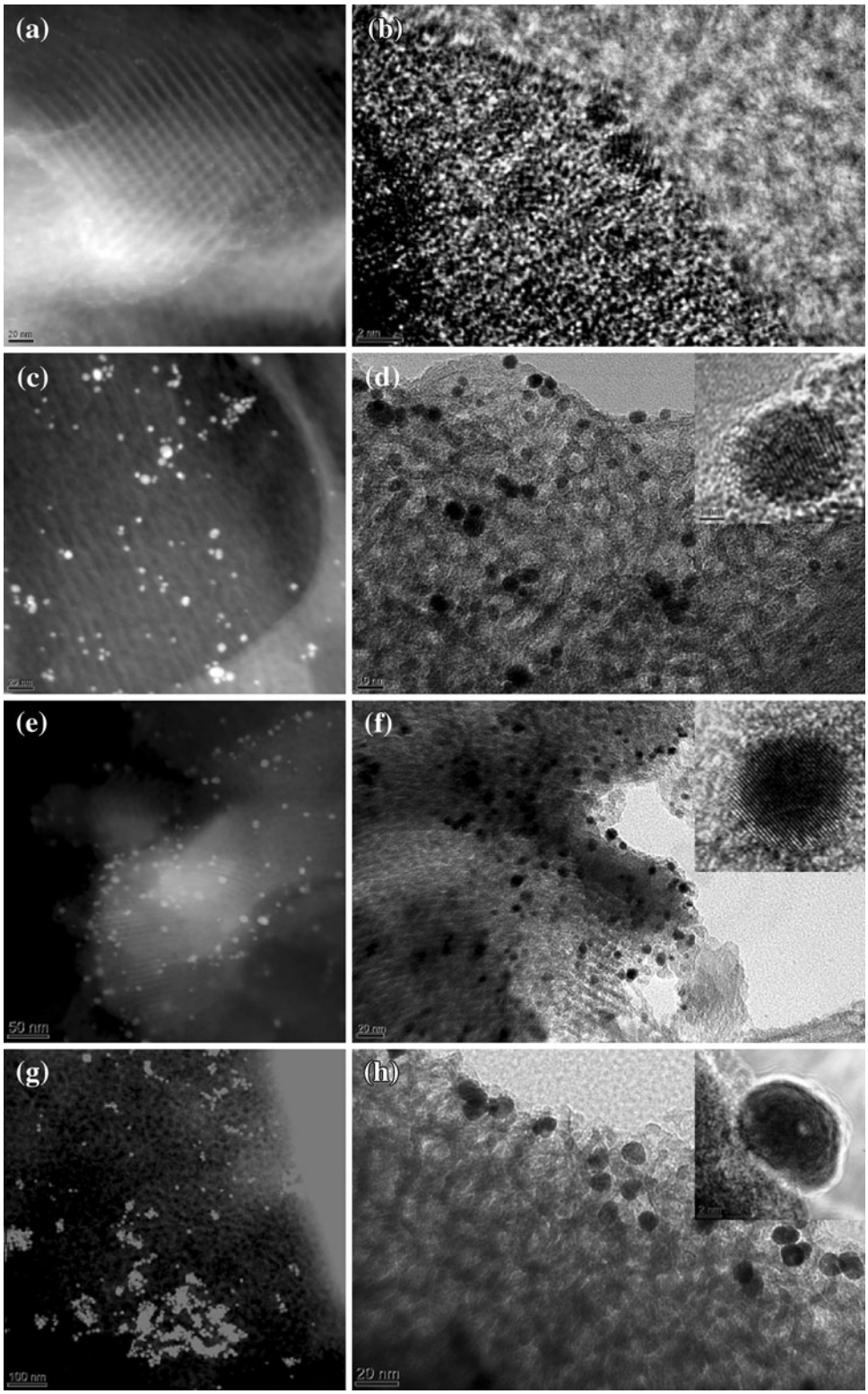

Fig. 1 Representative dark field and bright field TEM images of the post-MCP/H_2 reaction catalysts: **a**, **b** 1.5 nm Pt in SBA-15; **c**, **d** 3.0 nm Pt in SBA-15; **e**, **f** 5.2 nm Pt in SBA-15; and **g**, **h** 11.3 nm Pt in MCF-17. *Insets* show the HRTEM pictures

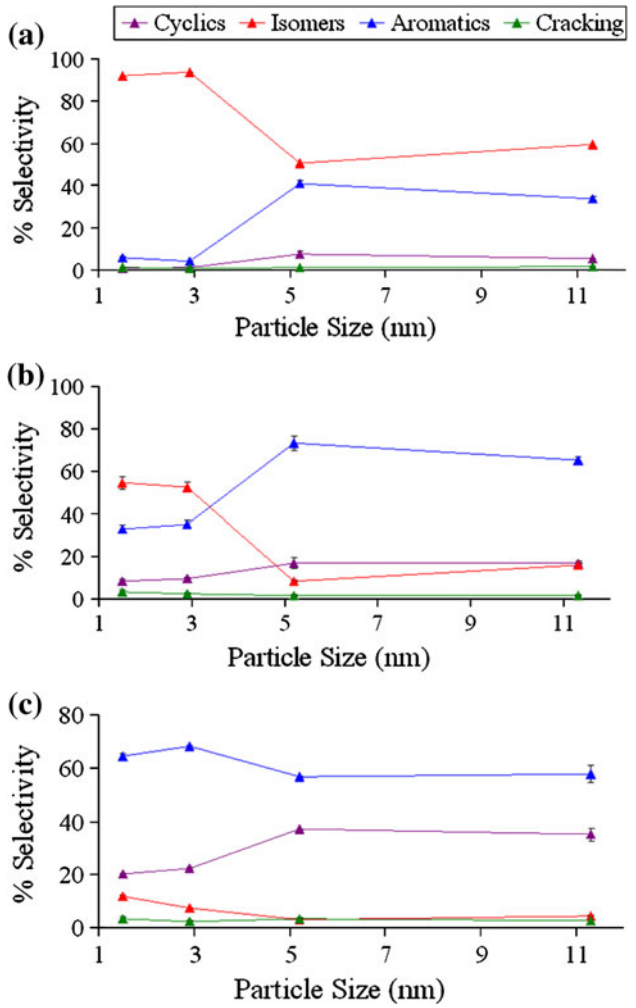

Fig. 2 Plots of % selectivity versus particle size for 50 Torr methylcyclopentane and 250 Torr H_2 at **a** 280 °C, **b** 320 °C and **c** 360 °C. Different reaction pathways are *color*-coded: *red* for isomerization, *blue* for aromatization, *purple* for cyclization and *green* for cracking

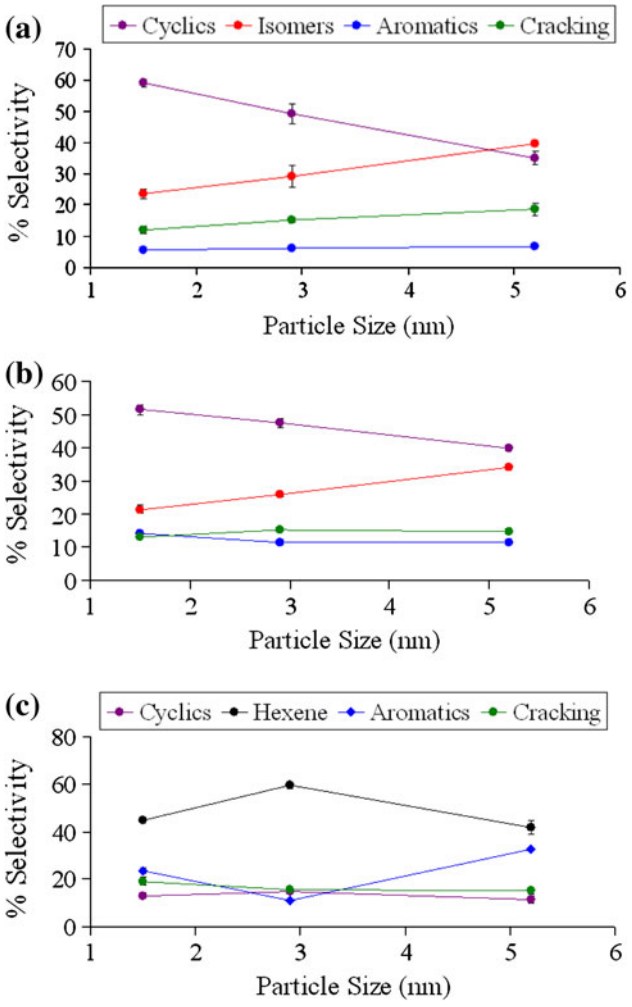

Fig. 3 Plots of % selectivity versus particle size for 50 Torr *n*-hexane and 250 Torr H_2 at **a** 280 °C, **b** 320 °C and **c** 360 °C. Different reaction pathways are *color*-coded as *red* for isomerization, *blue* for aromatization, *purple* for cyclization, *green* for cracking and *black* for dehydrogenation (to hexene)

different hydrocarbons respectively. No significant sintering was detected from the post-reaction TEM imaging of the catalysts, as shown in Fig. 1.

The selectivity for the MCP/H_2 reaction was shown in Fig. 2. Isomerization was the dominant reaction pathway for all Pt particle sizes at 280 °C. Small Pt nanoparticles, with mean size 3.0 nm and below, formed almost exclusively C_6-isomers under low operating temperature conditions (280 °C). Larger Pt nanoparticles, on the other hand, produced mixtures of C_6-isomers and benzene in comparable amounts at low temperatures (280 °C, Fig. 2a). At 320 °C, small Pt nanoparticles yielded C_6 isomers and benzene, isomerization remaining the dominant reaction pathway. However, for large Pt nanoparticles benzene was the major product at this temperature (Fig. 2b). At 360 °C aromatization became the main reaction pathway with a selectivity of greater than 55 % for all Pt particle sizes. Large Pt nanoparticles also led to the formation of methylcyclopentenes, whereas smaller Pt nanoparticles produced some C_6-isomers in addition to methylcyclopentenes (Fig. 2c). The selectivity for cracking hydrogenolysis stayed below 10 % for all Pt particle sizes and across all temperatures studied.

Next, we investigated the hydrogenative reforming of acyclic C_6 hydrocarbons to isolate the potential role of ring-opening products on the formation of benzene. It was found that there was only a weak particle size dependence and a minor temperature effect on the product selectivity for the reforming of acyclic C_6 hydrocarbons. Figure 3 shows the selectivity for the observed reaction pathways for the reforming of *n*-hexane, the linear C_6-isomer, at different temperatures. At 280 °C, the product distribution

showed only a weak particle size dependence. 1.5 nm Pt nanoparticles produced selectively more cyclics (60 % MCP) whereas 5.2 nm Pt nanoparticles more selectively isomerized *n*-hexane (~40 %) to 2-MP and 3-MP (Fig. 3a). Broadly speaking, the isomerization and cyclization pathways diminished upon increasing temperature to 360 °C in favor of dehydrogenation to hexene for all the particle sizes (Fig. 3c). Benzene production, on the other hand, slightly increased and hence reached ~30 % over 1.5 and 5.2 nm Pt nanoparticles. 3.0 nm Pt nanoaprticles, however, did not produce any significant fractions of benzene in the temperature range studied.

The reforming of 2-MP, a branched C_6 alkane, showed similar product distributions for different particle sizes, but did exhibit a strong particle size dependence on catalytic activity. C_5 cyclization to MCP (and methylcyclopentenes at 360 °C) was the main reaction pathway with almost invariably ~90 % selectivity at 280 °C and ~60 % selectivity at 360 °C (Fig. 4a, c). The 1.5 and 3.0 nm particles exhibited slightly higher selectivity towards C_6 isomerization than the 5.2 and 11.3 nm particles. Specifically, at 280 and 320 °C, *n*-hexane was the primary C_6 alkane produced, while 3-MP and/or dimethylbutanes were generated in higher yield at 360 °C. Benzene formation was less than 10 % at all temperatures studied.

Having provided a detailed description of the particle size dependent product distributions, we should discuss the relative turnover rates for the reforming of various C_6 hydrocarbons over size-controlled Pt nanoparticles, as this is equally important for a thorough assessment of the structure-sensitive hydrocarbon transformations over Pt. Figure 5 displays the plots of turnover rates versus mean Pt

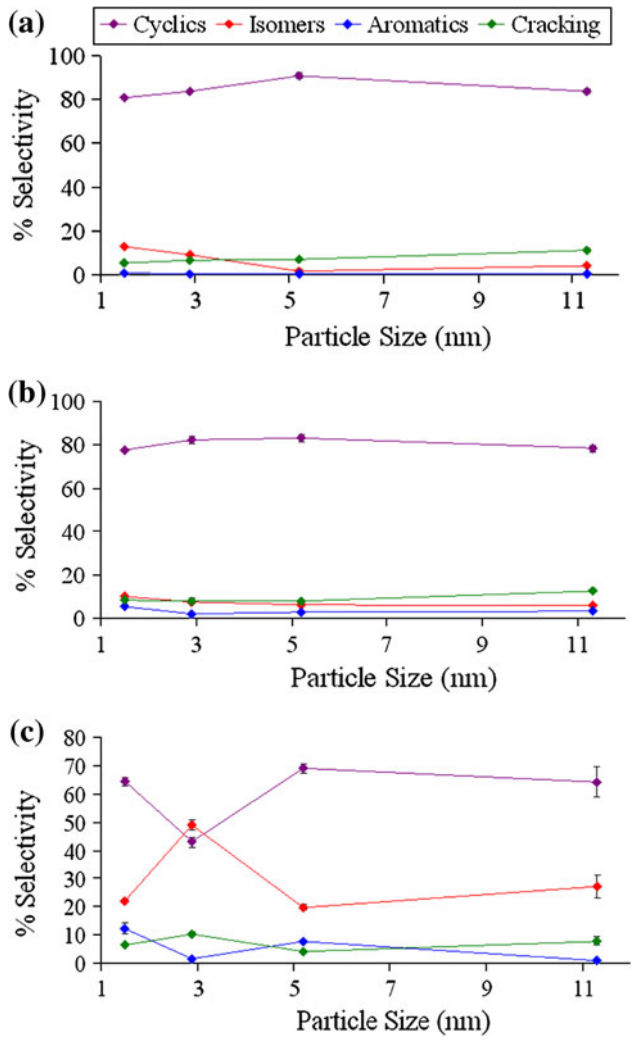

Fig. 4 Plots of % selectivity versus particle size for reaction of 50 Torr 2-methylpentane and 250 Torr H_2 at **a** 280 °C, **b** 320 °C and **c** 360 °C. Different reaction pathways are *color*-coded: *red* for isomerization, *blue* for aromatization, *purple* for cyclization and *green* for cracking

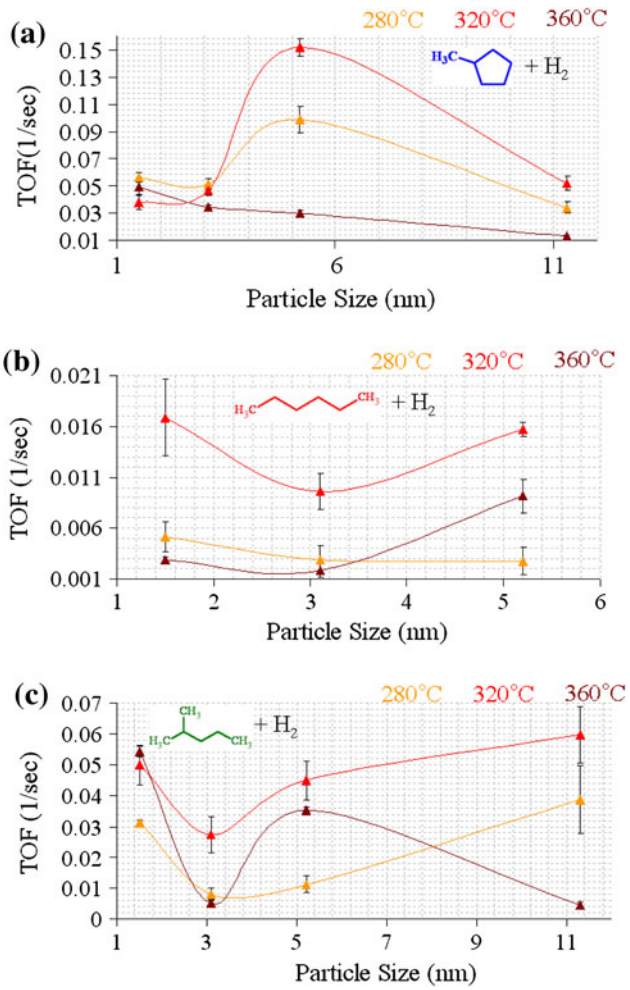

Fig. 5 Plots of turnover frequency versus size for the hydrogenolysis of **a** methylcyclopentane, **b** *n*-hexane and **c** 2-methylpentane. Temperatures are *color*-coded as *orange* for 280 °C, *red* for 320 °C and *brown* for 360 °C

nanoparticle sizes for the hydrogenative reforming of these C_6 hydrocarbons (MCP, 2-MP and *n*-hexane).

For the hydrogenolysis of MCP at 280 and 320 °C, 5.2 nm Pt nanoparticles exhibited a peak in activity over the other particle sizes by a factor of 3 in turnover rate. However, the turnover rate dropped monotonically from 0.05 s^{-1} for 1.5 nm Pt nanoparticles to 0.0013 s^{-1} for 11.3 nm Pt nanoparticles at 360 °C (Fig. 5a). It is important to note that the product distributions at 360 °C were significantly different from those at lower temperatures.

For the hydrogenative reforming of C_6 alkanes, 3.0 nm Pt nanoparticles performed poorly compared with the other particle sizes over the whole range of temperatures studied. The activity drop over 3.0 nm Pt nanoparticles was more pronounced for the hydrogenolysis of 2-MP, about an order of magnitude decrease compared to the 1.5 nm Pt nanoparticles at 360 °C (Fig. 5b). Similarly, the hydrogenolysis rate of *n*-hexane at 360 °C was slower over 3.0 nm Pt nanoparticles by a factor of 7 compared to 5.2 nm Pt nanoparticles and a factor of 4 compared to 1.5 nm Pt nanoparticles. Interestingly, 3.0 nm Pt nanoparticles were more selective for the isomerization of C_6 alkanes at 360 °C whereas the other particle sizes selectively led to cyclization and aromatization reactions under identical conditions.

4 Discussion

Our results for the hydrogenative reforming of various C_6 hydrocarbons over size-controlled Pt nanoparticles reveal measurable particle size effects. We have isolated a strong particle size dependence of the product distribution for the hydrogenolysis of MCP. Specifically, Pt nanoparticles size 3.0 nm and below selectively favored the hydrogenative ring opening and produced C_6 alkanes whereas large Pt nanoparticles size 5.2 nm and above yielded benzene via ring enlargement and aromatization. Furthermore, we have shown the impact of Pt particle sizes on the turnover rates along with selectivity for the reforming of C_6 alkanes, where 3.0 nm Pt nanoparticles were distinctly less active and yet more selective for the skeletal rearrangement to other C_6 isomers.

Our findings concerning the catalytic reactivity over monodisperse Pt nanoparticles in the 1.5–11.3 nm range are partly consistent with those that are reported in the literature. Paál and co-workers studied the n-hexane/H_2 reaction over regenerated 1.8 nm Pt/SiO_2 (EUROPT) and found that cyclization was the dominant reaction pathway (~43 %) followed by isomerization (~23 %) at 330 °C and 10 Torr hexane, 120 Torr H_2 [22]. They also detected some hydrogenolysis cracking products (~13 %) and benzene (~12 %) in agreement with our results for 50 Torr *n*-hexane and at 5:1 H_2 excess and 320 °C. Likewise, Chandler et al. [23] documented the selective formation of cyclic hydrocarbons over 3.0 nm Pt/SiO_2 for 49 Torr *n*-hexane and 200 Torr H_2 at 400 °C. These studies were carried out with Pt/SiO_2 catalysts that were not monodisperse. In our studies, using monodisperse catalysts, we have shown a marked difference between 1.5 and 5.2 nm Pt nanoparticles concerning the preferred reaction pathways under similar conditions (Fig. 3c).

The hydrogenolysis of 2-MP over unsupported Pt crystals and 3.0 nm Pt supported on alumina was reported by Garin et al. [24] at 350 °C and at very high H_2 excess (151:1). They found that cyclization was the main reaction pathway with selectivities in the range of 40–50 %. This is in good accord with our findings over 3.0 nm Pt nanoparticles at 360 °C and at 5:1 H_2 excess. However, a deviation from this observation was detected for the other monodisperse Pt nanoparticles as shown in Fig. 4c. Gault and co-workers [11] also reported the formation of 2,3-dimethylbutane during the hydrogenative reforming of 2-methylpentane over Pt films, which they attributed to a mechanism that involved a α, γ di-sigma adsorbed intermediate. In our studies for the reforming of 2-methylpentane, the selectivity for the formation of dimethylbutanes was only moderate (~10 %) even at elevated temperature, except the 11.3 nm Pt catalyst (i.e. large enough to be compared to bulk particle/film) which produced dimethylbutanes in significant fractions (~30 %) at 360 °C.

The hydrogenative reforming of C_6 hydrocarbons indicated a subtle dependence of catalytic reactivity on Pt nanoparticle sizes. To help assessing the reforming mechanism over Pt and to isolate the most likely reaction sites, we looked into a provisional correlation between the observed reactivity and size dependent surface coordination site distributions. For this purpose, we employed the methodology originally developed by Hardeveld and Hartog [25]. We used a modified cube-octahedron model, also described by Hardeveld and Hartog, for which (111) and (100) planes were covered by an extra layer of atoms, giving additional (110) and (311) planes. This way, we obtained model polyhedral clusters that mimic the as-synthesized nanoparticles as well as the post-reaction supported catalysts shown in Fig. 1. Then, coordination numbers (CNs) of surface atoms were calculated by using the magic number algorithms given in [25]. Corner sites were defined as surface atoms with CNs of 5 and 6, edge sites as those of 7 and 8, and terraces a coordination number of 9. The distributions of different surface sites for cluster sizes from 1.6 to 11.5 nm are depicted in Fig. 6. Based on this model, the spherical particles in the size range of 1.5–11.3 nm exhibit a constant fraction of edge sites (~0.3). More specifically, 1.5 nm particles possess the highest fraction of corner atoms, 3.0 nm particles have

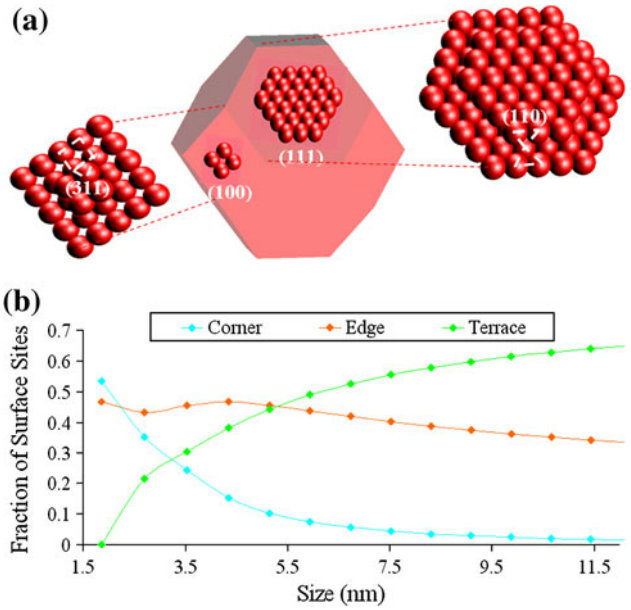

Fig. 6 **a** A modified cubo-octahedron cluster model showing the crystal faces with the extra atom planes superimposed in the [111] and [100] directions. **b** A plot of fraction of surface sites versus size for the modified cubo-octahedron cluster model

more edge atoms than corner and terrace atoms, while 5.2 nm particles possess the comparable fractions of edge and terrace atoms and 11.3 nm particles have terrace atoms maximized.

A tentative comparison between the observed catalytic reactivity and the calculated distribution of surface coordination sites shows similarities. First, small Pt nanoparticles size 3.0 nm and below would have higher fractions of corner and edge atoms and were catalytically more selective for the hydrogenative ring opening and isomerization reactions of MCP. Moreover, 3.0 nm Pt nanoparticles led to the isomerization of 2-MP and *n*-hexane more selectively than 1.5 nm Pt nanoparticles, yet they were the least active of all the particle sizes studied. Since the fraction of edge sites is broadly constant with varying particle size, the corner atoms are more likely to be the active catalytic sites for the isomerization of C_6 alkanes. Consistent with this hypothesis and our observations, Paal and co-workers [22, 26], with the aid of a morphological model proposed by Gnutzman and Vogel [27], attributed the isomerization of C_6 hydrocarbons to the presence of corner and edge sites. A sextet mechanism was proposed by Balandin [28], who predicted 6-atom (111) planes as the active sites for aromatization. Consistent with this, we found Pt nanoparticles with large fractions of terrace atoms provided active catalytic sites for the ring enlargement and dehydrogenolysis of MCP. However, 1.5 nm Pt nanoparticles led to the ring closure and dehydrogenation of 2-MP and *n*-hexane in fractions comparable to that over the 5.2 nm Pt nanoparticles. This suggests a different reaction mechanism operative for the aromatization of C_6 hydrocarbons over the 1.5 nm Pt.

Finally, the peculiar deactivation of these size-controlled Pt nanoparticles for the hydrogenolysis of C_6 hydrocarbons at high temperatures can tentatively be attributed to the deposition of carbonaceous species from hydrocarbons during reaction. This is supported by the absence of particle sintering after reaction (Fig. 1) and the known effects of temperature and hydrogen partial pressure on the loss of Pt surface area during catalytic hydrocarbon transformations [29]. We previously documented that the regeneration of the size-controlled Pt nanoparticles by redox cycles at 150 °C could restore about 70 % of the initial catalytic activity for the hydrogenolysis of MCP (1:5 MCP:H_2) at 340 °C. This suggests that the deactivation is at least in part due to surface accumulation of hydrocarbon deposits. It was proposed that the deactivation was correlated with an increase in the production of C_5-cycloalkenes. For the MCP/H_2 reaction, we found correlations with Pt nanoparticle size both for the formation of C_5-cycloalkenes and for the deactivation rates.

5 Conclusion

Our systematic studies for the hydrogenative reforming of various C_6 hydrocarbons over the model Pt nanoparticle catalysts have isolated particle sizes around 3.0 nm as the most active for the formation of C_6 isomers. 3.0 nm Pt nanoparticles yielded C_6 isomers more selectively than any other particle size (50 % vs. a maximum of 20 %) for the 2-methylpentane/H_2 reaction at 360 °C. Yet the turnover rates for the reforming of C_6 alkanes over 3.0 nm Pt nanoparticles were an order of magnitude slower than those over 1.5 and 5.2 nm Pt. Similarly, for the hydrogenolysis of MCP at 320 °C, Pt particle sizes of 3.0 nm and below produced C_6 isomers more selectively than benzene whereas the larger Pt nanoparticles were more selective for the formation of benzene.

Acknowledgments This work is funded by Office of Science, Department of Energy (DOE-BES) and Chevron Corporation. Nanoparticle imaging was performed at the Molecular Foundry and the National Center for Electron Microscopy, Lawrence Berkeley Lab, which is supported by the US Department of Energy under Contract # DE-AC02-05CH11231.

References

1. Kuhn JN, Tsung CK, Huang W, Somorjai GA (2009) J Catal 265:209–215
2. Tsung CK, Kuhn JN, Huang WY, Aliaga C, Hung LI, Somorjai GA, Yang PD (2009) J Am Chem Soc 131:5816–5822

3. Kuhn JN, Huang WY, Tsung CK, Zhang YW, Somorjai GA (2008) J Am Chem Soc 130:14026
4. Kliewer CJ, Aliaga C, Bieri M, Huang WY, Tsung CK, Wood JB, Komvopoulos K, Somorjai GA (2010) J Am Chem Soc 132:13088–13095
5. Narayanan R, El-Sayed MA (2004) Nano Lett 4:1343–1348
6. Zaera F, Godbey D, Somorjai GA (1986) J Catal 101:73–80
7. Garin F, Aeiyach S, Legare P, Maire G (1982) J Catal 77:323–337
8. Brandenberger SG, Callender WL, Meerbott WK (1976) J Catal 42:282–287
9. Zhuang YP, Frennet A (1999) Appl Catal A Gen 177:205–217
10. Galperin LB, Bricker JC, Holmgren JR (2003) Appl Catal A Gen 239:297–304
11. Barron Y, Maire G, Muller JM, Gault FG (1966) J Catal 5:428–446
12. Dautzenberg FM, Platteeuw JC (1970) J Catal 19:41–48
13. Bai XL, Sachtler WMH (1991) J Catal 129:121–129
14. Davis BH (1999) Catal Today 53:443–516
15. Teschner D, Paal Z, Duprez D (2001) Catal Today 65:185–190
16. Samoila P, Boutzeloit M, Especel C, Epron F, Marecot P (2009) Appl Catal A Gen 369:104–112
17. Poupin C, Pirault-Roy L, La Fontaine C, Toth L, Chamam M, Wootsch A, Paal Z (2010) J Catal 272:315–319
18. Vaarkamp M, Dijkstra P, Vangrondelle J, Miller JT, Modica FS, Koningsberger DC, Vansanten RA (1995) J Catal 151:330–337
19. Kramer R, Fischbacher M (1989) J Mol Catal 51:247–259
20. Anderson JBF, Burch R, Cairns JA (1987) J Catal 107:351–363
21. Alayoglu S, Aliaga C, Sprung C, Somorjai GA (2011) Catal Lett 141:914–924
22. Bond GC, Paál Z (1992) Appl Catal A Gen 86:1–35
23. Chandler BD, Rubinstein LI, Pignolet LH (1998) J Mol Catal A Chem 163:43–53
24. Garin F, Girard P, Maire G, Lu G, Guczi L (1997) Appl Catal A Gen 152:237–247
25. Hardeveld RV, Hartog F (1969) Surf Sci 15:189–230
26. Paál Z (1992) Catal Today 12:297
27. Gnutzman V, Vogel W (1990) J Phys Chem 94:4991
28. Balandin AA (1969) Adv Catal 19:1
29. Bond GC, Lin X (1997) J Catal 168:207–216